THE JOURNAL OF PHYSICAL CHEMISTRY A

Article

pubs.acs.org/JPCA

O_2^-·[Polar VOC] Complexes: H-Bonding versus Charge–Dipole Interactions, and the Noninnocence of Formaldehyde

Kellyn M. Patros,[†] Jennifer E. Mann,[‡] and Caroline Chick Jarrold*[,†]

[†]Department of Chemistry, Indiana University, 800 East Kirkwood Avenue, Bloomington, Indiana 47405, United States

[‡]Physical Electronics, 18725 Lake Drive East, Chanhassen, Minnesota, 55317, United States

Supporting Information

ABSTRACT: Anion photoelectron imaging was used to measure the photodetachment spectra of molecular complexes formed between O_2^- and a range of atmospherically relevant polar molecules, including species with a carbonyl group (acetone, formaldehyde) and alcohols (ethanol, propenol, butenol). Experimental spectra are analyzed using a combination of Franck–Condon simulations and electronic structure calculations. Strong charge–dipole interactions and H-bonding stabilize the complex anions relative to the neutrals, resulting in a *ca.* 1 eV increase in electron binding energy relative to bare O_2^-, an effect more pronounced in complexes with H-bonding. In addition, broken degeneracy of the O_2-local π_g orbitals in the complexes results in the stabilization of the low-lying excited O_2 (a $^1\Delta_g$)·[polar VOC] state relative to the ground O_2 ($X\ ^3\Sigma_g^-$)·[polar VOC] state when compared to bare O_2. The spectra of the O_2^-·[polar VOC] complexes exhibit less pronounced laser photoelectron angular distribution (PADs). The spectrum of O_2^-·formaldehyde is unique in terms of both spectral profile and PAD. On the basis of these experimental results in addition to computational results, the complex anion cannot be described as a distinct O_2^- anion partnered with an innocent solvent molecule; the molecules are more strongly coupled through charge delocalization. Overall, the results underscore how the symmetry of the O_2 π_g orbitals is broken by different polar partners, which may have implications for atmospheric photochemistry and models of solar radiation absorption that include collision-induced absorption.

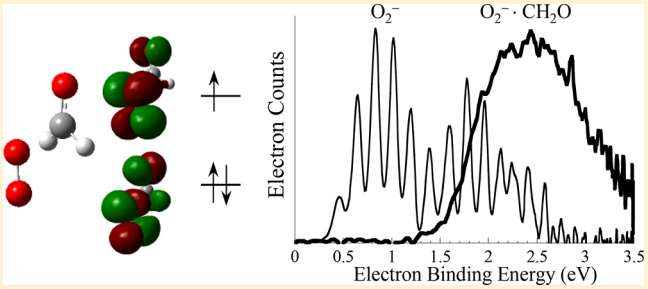

I. INTRODUCTION

The importance of molecular oxygen in the atmosphere cannot be overstated. O_2 participates in numerous atmospheric chemical and physical processes when undergoing molecular collisions, including collision-induced absorption[1−10] and photosensitization.[11−15] We recently reported the results of a study of neutral O_2·VOC (VOC = hexane, isoprene, benzene, and benzene-d_6) collision complexes by photoelectron imaging (PEI) spectroscopy of the anionic precursor.[16] Photodetachment of the anionic complex prepares the neutrals on a repulsive region of the O_2–VOC intermolecular potential energy surface. Our results showed that the O_2 (a $^1\Delta_g$)·VOC lifetimes and energy relative to the O_2 ($X\ ^3\Sigma_g^-$)·VOC ground electronic state varied with VOC identity. The work presented herein is an extension of the previous study[16] to polar VOCs containing an alcohol or a carbonyl substituent group.

We have selected a range of polar VOC collision partners with relevance in atmospheric chemistry and to provide a point of comparison to our previous study that included several unsaturated nonpolar collision partners. Formaldehyde is an atmospherically important carcinogen[17] that is a common byproduct of numerous VOC oxidation reactions,[18] and subsequently forms radicals[19,20] that contribute to tropospheric ozone formation.[21,22] Acetone is primarily formed by terrestrial vegetation and (anthropogenic) isoalkanes[23−25] and offers a methylated analog for comparison to formaldehyde. Ethanol (EtOH) not only supplements the automobile fuel supply[26−28] but also poses health threats,[29] and its atmospheric sources and sinks are not well-understood.[30,31] Oxygenated VOCs such as 2-propenol (allyl alcohol), 3-buten-1-ol, and 3-buten-2-ol are largely anthropogenic[32,33] and lead to secondary aerosol formation.[34]

A significant difference between the O_2^-·[polar VOC] complexes in the current study and the O_2^-·[nonpolar VOC] complexes studied previously[16] arises from the strong charge–dipole interactions and hydrogen bonding that favor a distinct structural orientation between the O_2^- anion and the neutral VOC. In the case of nonpolar partners, the intermolecular potential energy surface was inferred to be flat, on the basis of the numerous close-lying structural minima separated by low barriers found computationally. The anion PEI spectra of these complexes therefore were assumed to reflect an ensemble of intermolecular orientations that were nearly identical in energy. In contrast, photodetachment of O_2^-·[polar VOC] will have Franck–Condon overlap with a specific orientation between the resulting neutral molecules. The results of the current study

Received: May 26, 2017
Revised: June 30, 2017
Published: July 3, 2017

DOI: 10.1021/acs.jpca.7b05124
J. Phys. Chem. A 2017, 121, 5459−5467

shed light on the differences in interaction energy for systems with a large dipole but weak C−H hydrogen bonding versus alcohols with both O−H and C−H hydrogen bonding. We also find that the broken degeneracy of the O_2-local π_g orbitals results in a stabilization of the O_2 (a $^1\Delta_g$)·[polar VOC] excited neutral state relative to the ground O_2 (X $^3\Sigma_g^-$)·[polar VOC] state. The PE spectrum of O_2^-·formaldehyde is unique in both profile and photoelectron angular distribution. The experimental and computational results suggest interesting electronic coupling between O_2^- and formaldehyde.

II. METHODS

II.A. Experimental Details. The anion photoelectron imaging apparatus has been described elsewhere;[35] therefore, a brief description follows. Mixtures of O_2 and room temperature polar VOC (formaldehyde, acetone, EtOH, 2-propenol, 3-buten-1-ol, 3-buten-2-ol) (60 psig) were coexpanded by using a pulsed molecular beam valve through a needle electrical discharge.[36] The gas mixture passed through a skimmer, and the anions were accelerated to 1 keV. The ions were re-referenced to ground potential in a high-voltage switch[37] before entering a time-of-flight mass spectrometer.[38,39]

Prior to colliding with a dual microchannel plate detector assembly, the anions of interest were selectively photodetached using the third harmonic (3.495 eV) output of a Nd:YAG laser (Continuum Surelite, 30 Hz). Photoelectrons were extracted using a velocity map imaging lens system,[40] and images are recorded on a dual microchannel plate-phosphor screen detector with a CCD camera.[41,42] Three-dimensional PE velocity distributions are obtained using BASEX[43] and then converted to electron kinetic energy (e^-KE). Photoelectron spectra are plotted as a function of electron binding energy, $e^-BE = h\nu - e^-KE$, which is independent of photon energy. A Jacobian velocity to energy transformation was performed $[I(e^-KE) \propto I(v)/v$, where v is the electron velocity, proportional to the image radius] on all of the spectra shown. Calibrations based on the well-known PE spectrum of O_2^- were performed for each complex.[44] The pBASEX code[45] was used to produce images with fewer artifacts on the polarization axis line compared to BASEX.

II.B. Computational Details. Though open-shell species are more appropriately treated with higher levels of theory, more modest levels of theory are practical for the size of the molecular complexes in this study. Multiple initial structures for each anion and neutral O_2·[polar VOC] complex were explored by using the GAUSSIAN09 program suite for electronic structure calculations.[46] Optimized geometries were calculated at the second-order Moller−Plesset perturbation (MP2) level of theory with the cc-pVDZ basis set followed by MP2/aug-cc-pVTZ single-point calculations.[47] Diffuse functions were added to all atomic centers (s and p functions) using an exponent ratio of 0.3 to maintain even-tempered basis set behavior.[48] Frequency calculations were performed to verify that global minima were found. All of the relative optimized energies reported are zero-point corrected. In addition, vertical detachment transition energies were calculated by the difference in energy between the optimized anion and single point calculation on the neutral confined to the anion geometry. We note here that basis set superposition error (BSSE) corrections in comparable systems[49,50] are on the order of several millielectronvolts for neutrals. In our own calculations on O_2^-·isoprene along with the triplet and singlet neutrals BSSE correction energies ranged from 0.02 eV for the triplet neutral to 0.05 eV for the anion and singlet neutral. Because we are interested in the relative energies of O_2^-·[polar VOC] and O_2 (X $^3\Sigma_g^-$ and a $^1\Delta_g$)·[polar VOC] measured with fairly low resolution (*vide infra*), we do not include BSSE corrections.

III. RESULTS AND ANALYSIS

III.A. O_2^-·[polar VOC]; VOC = Acetone and Alcohols. The PEI spectra of bare O_2^- and O_2^-·[polar VOC] (polar VOC = acetone, EtOH, 2-propenol, 3-buten-1-ol, and 3-buten-2-ol, and formaldehyde) measured using 3.493 eV photon energy are shown in Figure 1. The raw and reconstructed

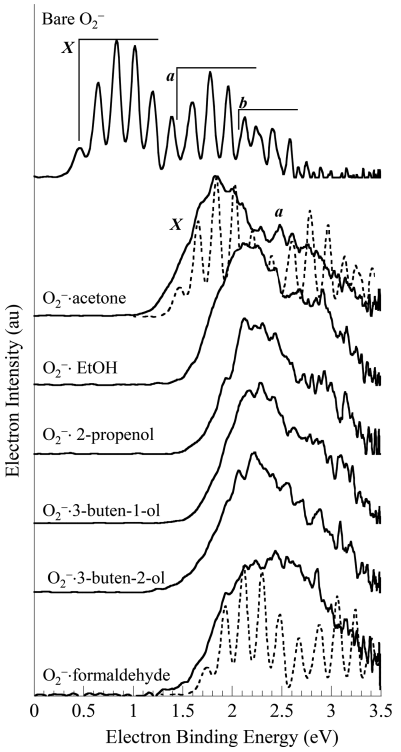

Figure 1. PE spectra of O_2^- and O_2^-·[polar VOC] complexes obtained using 3.49 eV photon energy. Raw and reconstructed photoelectron images are included in the Supporting Information.

images are included in the Supporting Information. The O_2^- PE spectrum is well-known[44] and exhibits transitions to the X $^3\Sigma_g^-$, a $^1\Delta_g$, and b $^1\Sigma_g^+$ neutral electronic states from the X $^2\Pi_g$ anion ground state, the origins of which are indicated in Figure 1. Spectra of the O_2^-·[polar VOC] complexes all feature a prominent band X comparable in overall profile to band X in the bare O_2^- spectrum, with the exception of O_2^-·formaldehyde. The PE spectrum of bare O_2^- shifted to higher binding energy is superimposed as a dashed trace on the spectra of O_2^-·acetone and O_2^-·formaldehyde to underscore the different profile observed for band X of the O_2^-·formaldehyde compared to the other spectra. Additional spectral disparities will be explained below.

All of the O_2^-·[polar VOC] spectra are shifted to *ca.* 1 eV higher e^-BE values compared to the bare O_2^- spectrum, which is similar to what was observed in the PEI spectrum of the simpler charge−dipole O_2^-·H_2O complex.[51] The vertical detachment energies for all spectra are summarized in Table 1. Assuming the charge is localized on O_2^- and that the polar VOC partner remains in its S_0 ground electronic state, the increase in binding energy is primarily due to the stabilization

DOI: 10.1021/acs.jpca.7b05124
J. Phys. Chem. A 2017, 121, 5459−5467

Table 1. Summary of O_2^- and O_2^-·[polar VOC] Spectral Band Positions (Figure 1), Asymmetry Parameters, and Origins of Spectral Simulations Shown in Figures 3 and 4[a]

	exptl VDE (eV)	β	simulation origins (eV)[b]	scaling factor for band a
O_2^-				
X	0.82	−0.8	0.448	
a	1.78	−0.6	1.425 (T_0 = 0.977)	1
b	2.40		2.075 (T_0 = 1.627)	
O_2^-·acetone				
X	1.76(3)	−0.42	1.32	
a	2.62(5)		2.15 (T_0 = 0.83)	0.82
O_2^-·EtOH				
X	2.11(5)	−0.39	1.55	
a	2.8(1)		2.31 (T_0 = 0.76)	0.75
O_2^-·propenol				
X	2.23	−0.44		
a	2.9(1)			
O_2^-·3-buten-1-ol				
X	2.23	−0.40		
a	2.9(1)			
O_2^-·3-buten-2-ol				
X	2.19(5)	−0.34	1.68	
a	2.9(1)		2.41 (T_0 = 0.72)	0.62
O_2^-·formaldehyde				
X	2.1−2.7	+0.3	1.57	
a			2.23 (T_0 = 0.64)	1.2

[a]The scaling factor for band a was set by assuming band X in the complex spectra and the bare O_2^- spectra had the same intensity and then scaling band a in the complex spectra relative to band a in the bare O_2^- spectrum to achieve overall agreement between the experimental and simulated spectra. [b]The origins for the O_2^- spectral simulation are from the known neutral state term energies and electron affinity summarized in ref 44. The origins for the remaining spectral simulations were set to match the experimental vertical detachment energy.

of the anion by charge−dipole interactions and also may have contributions from repulsion on the neutral potential, as illustrated in Figure 2. On the basis of the size of this shift in e^-BE, as indicated in Figure 2, the PE spectra of the complexes should exhibit transitions to the O_2 ($X\ ^3\Sigma_g^-$)·[S_0] and O_2 ($a\ ^1\Delta_g$)·[S_0] neutral states, with the O_2 ($b\ ^1\Sigma_g^+$)·[S_0] state becoming energetically inaccessible with 3.493 eV photon energy. As with previously reported spectra of O_2^- complexes,[16,51−53] the O_2 vibrational progression is not resolved due to neutral dissociation, activation of low-frequency intermolecular modes and low-frequency modes localized on the complex partner.

In contrast to our previously reported spectra on complexes formed between O_2^- and nonpolar VOC's,[16] band a in the O_2^-·[polar VOC] spectra appears as a lower-intensity shoulder on high-e^-BE side of band X in the spectrum, or in the case of O_2^-·3-buten-2-ol, it is indistinguishable from band X. In an effort to quantify this effect, spectral simulations were performed on several of the spectra in the following manner. First, we set our simulation code to reproduce the relative intensities of the transitions observed in the PE spectrum of bare O_2^- measured with our experimental apparatus, using well-known spectroscopic parameters,[44] shown in Figure 3a. A low-frequency mode was then introduced to the O_2 vibrational progression (in all cases, ω' = 200 cm^{-1}, ω'' = 170 cm^{-1}, ΔQ = 1.5 Å·$amu^{1/2}$) to broaden the peaks to approximate the appearance of the bands in the O_2^-·[polar VOC] spectra, and the position and relative intensities of the broadened bands X and a were adjusted so that their sum matched the general profile of the O_2^-·[polar VOC] spectra. We applied this procedure to simulate the PE spectra of O_2^-·acetone, O_2^-·EtOH, and O_2^-·3-buten-2-ol, the results of which are shown in Figure 3b−d. The origins of bands X and a used to generate the simulations of these spectra are summarized in Table 1. For all the simulations, we set the maximum intensity of band X at a constant and then scaled band a relative to band a in the bare O_2^- spectrum. This scaling factor is also included in Table 1.

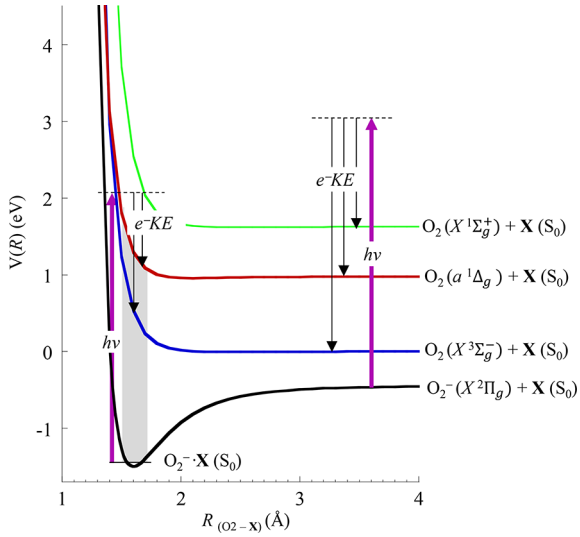

Figure 2. Energy level diagram showing how (i) the measured electron binding energy increases for O_2^-·[polar VOC] complex anions relative to O_2^- due to enhanced stability of anion in addition to Franck−Condon overlap with a repulsive part of the neutral potential and (ii) the neutral O_2 ($b\ ^1\Sigma_g^+$)·[polar VOC] becomes energetically inaccessible via photodetachment of O_2^-·[polar VOC] with 3.49 eV photon energy.

Though the intensities at every point in the PE spectra of the O_2^-·[polar VOC] spectra are not matched exactly (for example, the slope of the low-e^-BE edge of band X in the O_2^-·3-buten-2-ol), the qualitative profiles and partially resolved shoulder-like O_2 stretch progressions align with the experimental spectra in all three simulations (Figure 3b−d). Included on the simulation panels are the increase in binding energy (ΔEA) introduced to match the simulated and experimental vertical detachment energy of band X and the term energy of the O_2 ($a\ ^1\Delta_g$) or O_2 ($a\ ^1\Delta_g$)·[polar VOC] state used in the simulation of band a.

A general trend of increasing EA and lower-term energy of the $a\ ^1\Delta_g$·[S_0] state in the complexes evident from the simulations is borne out to some extent in the results of calculations on these complexes, summarized in Table 2. Though all of the calculations underestimate the adiabatic EA of bare O_2 and its complexes, the increases in calculated adiabatic EA of the complexes relative to bare O_2 shadow the observed shifts in the spectra. The EA of O_2·acetone is calculated to be 0.71 eV higher than the EA of O_2, whereas experimentally, the difference is approximated as 0.88 eV on the basis of the simulated match to the band X maximum (note that the manner in which the simulations were implemented accounts for low Franck−Condon intensity near the origin due to activation of low-frequency modes in the complex). For O_2·EtOH, the calculated EA is 0.93 eV higher, compared to the

DOI: 10.1021/acs.jpca.7b05124
J. Phys. Chem. A 2017, 121, 5459−5467

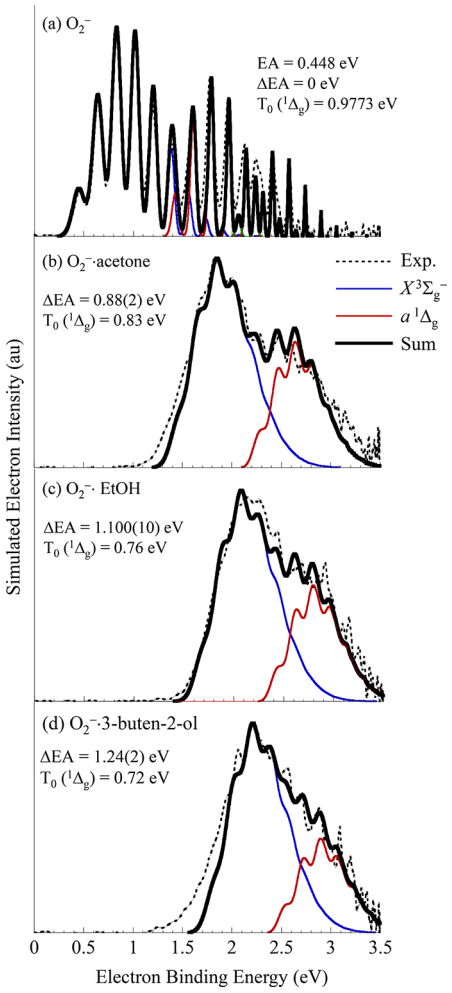

Figure 3. Simulation of the (a) O_2^- PE spectrum used in generating the simulations of the O_2^-·[polar VOC] complex spectra (b)−(d). ΔEA is the energy difference between the origins of the bare O_2^- and O_2^-·[polar VOC] complex simulations of band X. T_0 ($^1\Delta_g$) is the energy difference between the origins of the simulation of band a and the simulation of band X.

approximate experimental shift of 1.10 eV. The largest calculated increase in EA for the complexes were found for both the O_2·3-butenol complexes, 1.03 eV (experimentally, a shift of 1.24 eV was approximated from the spectrum of O_2^-·3-buten-2-ol). At the same time, the calculated term energies of the O_2 (a $^1\Delta_g$)·[polar VOC] complexes were calculated to be lower in energy than the calculated bare O_2 a $^1\Delta_g$ state, by approximately 0.1−0.15 eV.

The increases in EA do not track the magnitude of the permanent dipole moments of the polar partners. Acetone has the largest dipole moment of the molecules in this series, 2.91 D, whereas the alcohols have dipole moments ranging from 1.6 to 1.9 D, with formaldehyde having an intermediate dipole moment of 2.33 D.[54] The distance between the O_2^- charge and the acetone dipole is sterically limited by the methyl groups in acetone in the O_2^-·acetone complex, and the interaction lacks the intimate proximity anticipated for the hydrogen bonding available with the alcohols. Additional stabilization of the anion may also be due to the polarizability of the partner molecules, as is evident from the modest increase in EA with the larger alcohols relative to EtOH.

Figure 4 shows representative structures that converged in calculations on the O_2·acetone complex anion and neutrals, along with the most stable structures found for O_2^-·EtOH and O_2^-·3-buten-2-ol. Structures from all calculations that converged, along with calculated relative energies, are included in the Supporting Information. O_2^-·acetone is unique in that three distinct but nearly isoenergetic minima converged in calculations, all with O_2^- situated at the positive end of the acetone dipole moment. Hypothetical photodetachment transitions from any of these three anion structures are predicted to be at e^-BE = 0.98−1.00 eV for the triplet neutral and e^-BE = 2.23−2.27 eV for the singlet neutral. In the case of the O_2^-·alcohol complexes, one distinct structure emerged as the most stable and was generally 0.5 eV lower in energy than the next most stable structure. As with the O_2^-·ethanol and O_3^-·3-buten-2-ol structures shown in Figure 4, the O_2^- molecule forms a conventional H-bond with the hydroxyl group, and a C−H hydrogen bond with an H-atom on the β-carbon. The transition energies summarized in Table 2 are based on transitions from the lowest energy isomer of the anion to the neutral isomers that are most structurally similar. As in previous studies, the neutral intermolecular surface is flat, with numerous different isomers converging with very similar energies.

III.B. O_2^-·Formaldehyde. As noted above, the profile of the O_2^-·formaldehyde spectrum is qualitatively different from the other complex spectra presented above. In addition, the photoelectron angular distribution (PAD) observed in the PEI collected for O_2^-·formaldehyde is also qualitatively different. For a randomly oriented species, the differential cross section is given by[55]

$$\frac{\partial\sigma}{\partial\Omega} = \frac{\sigma_{\text{total}}}{4\pi}\left[1 + \beta(E)\left(\frac{3}{2}\cos^2\theta - \frac{1}{2}\right)\right] \quad (1)$$

where σ_{total} is the total photodetachment cross section, and $\beta(E)$ is an electron kinetic energy-dependent asymmetry parameter ranging from −1 for perpendicular transitions to +2 for parallel transitions. Mabbs and co-workers[56] have shown $\beta(E)$ ranges from −0.7 to −1 for the O_2^- photodetachment transitions in the range of e^-KE values sampled in this study [the molecular orbital associated with the detachment transition has $\lambda = \pm 1$, resulting in interference between $l = 0$, 2 photoelectrons, with $l = 0$ becoming more predominant at lower e^-KE resulting in $\beta(E)$ approaching zero].

Figure 5a shows the reconstructed PEIs obtained for O_2^- and O_2^-·formaldehyde, along with a plot of the relative intensities of the most intense portion of band X in all of the spectra, shown in Figure 5b. Plots showing slices through the reconstructed images at 10° increments are in the Supporting Information (Figure S2). The PEI of O_2^- shows the clear perpendicular PAD ($\beta = -0.8$) in agreement with Mabbs et al., whereas the PAD of O_2^-·formaldehyde is more parallel ($\beta = +0.3$). The asymmetry parameters for all the spectra are included in Table 1. Except for O_2^-·formaldehyde, $\beta \approx -0.4$ for all of the complex spectra, whereas for bare O_2^- at comparable electron kinetic energy (e^-KE ≈ 1 eV), Mabbs reported an asymmetry parameter of −0.8.

An attempt to simulate the O_2^-·formaldehyde spectrum using the same approach applied to simulating the spectra presented above is shown in Figure 5c. Although the unique profile of the spectrum can be qualitatively reproduced by assuming overlapping transitions to the X $^3\Sigma_g^-$·[S_0] and a $^1\Delta_g$·

DOI: 10.1021/acs.jpca.7b05124
J. Phys. Chem. A 2017, 121, 5459−5467

Table 2. O_2 Bond Lengths Determined from MP2/cc-pVDZ Optimized Structures, with the Relative Energies from MP2/aug-cc-pVTZ Single-Point Calculations on the MP2/cc-pVDZ Optimized Structures, and Vertical Detachment Energies[b]

	calcd rel energy (eV)	calcd T_0 (a $^1\Delta_g$, eV)	r(O−O) (Å)	calcd VDE (eV)	exp VDE (eV)
O_2 ($^1\Delta_g$)	1.56 (1.425)	1.33 (0.9773)	1.259 (1.216)	1.62	1.78
O_2 ($^3\Sigma_g^-$)	0.29 (0.448)		1.232 (1.208)	0.49	0.82
O_2^- ($^2\Pi_g$)	0		1.373 (1.348)		
O_2 ($^1\Delta_g$)·acetone	2.26	1.26	1.259	2.81	2.62
O_2 ($^3\Sigma_g^-$)·acetone	1.00		1.233	1.78	1.76
O_2^- ($^2\Pi_g$)·acetone	0		1.353		
O_2 ($^1\Delta_g$)·EtOH	2.41	1.19	1.259	2.88	2.8
O_2 ($^3\Sigma_g^-$)·EtOH	1.22		1.223	1.85	2.11
O_2^- ($^2\Pi_g$)·EtOH	0		1.317		
O_2 ($^1\Delta_g$)·propenol	2.55	1.28	1.258	3.04	2.9
O_2 ($^3\Sigma_g^-$)·propenol	1.35		1.224	2.05	2.23
O_2^- ($^2\Pi_g$)·propenol	0		1.317		
O_2 ($^1\Delta_g$)·3-buten-1-ol	2.56	1.24	1.258	3.06	2.9
O_2 ($^3\Sigma_g^-$)·3-buten-1-ol	1.32		1.224	[a]	2.23
O_2^- ($^2\Pi_g$)·3-buten-1-ol	0		1.320		
O_2 ($^1\Delta_g$)·3-buten-2-ol	2.54	1.22	1.258	3.03	2.90(5)
O_2 ($^3\Sigma_g^-$)·3-buten-2-ol	1.32		1.225	2.04	2.20(3)
O_2^- ($^2\Pi_g$)·3-buten-2-ol	0		1.317		
O_2 ($^1\Delta_g$)·formaldehyde	2.37	1.23	1.260	3.14	
O_2 ($^3\Sigma_g^-$)·formaldehyde	1.14		1.229	2.25	2.1−2.7
O_2^- ($^2\Pi_g$)·formaldehyde	0		1.301		

[a]The single-point calculation on the O_2 ($^3\Sigma_g^-$)·3-buten-1-ol VDE yielded a nonphysical value of 3.07 eV, which is not in line with the other complexes studied here. [b]Values in parentheses are experimental values from ref 44.

[S_0] states, the simulation also highlights the fairly high experimental electron signal intensity electron at very low e^-KE (high e^-BE), which is another distinguishing feature of the O_2^-·formaldehyde complex. Overall, the experimental evidence suggests that the complex cannot be described as a distinct O_2^- anion in a molecular complex with formaldehyde. Rather, the constituent molecules are electronically coupled; formaldehyde is not an innocent neutral partner.

This experimental result is also borne out in the computational results. Figure 6 contrasts the delocalized singly occupied HOMO and doubly occupied HOMO−1 of the O_2^-·formaldehyde complex with the O_2^--local molecular orbitals of the O_2^-·EtOH complex, the latter of which is typical of all of the other complexes studied here. In addition, the charge on the O_2^- portion of O_2^-·formaldehyde is less negative than in the other complexes, and the calculated C═O bond in formaldehyde is elongated by ca. 0.03 Å relative to the calculated C═O bond length in the neutral complex. The O—O bond length in the anion is also calculated to be shorter than the O—O bond length in all of the other complex anions, as summarized in Table 2, reflecting lower occupancy of the O_2-local π_g orbital. Additional structural details from the calculations are included in the Supporting Information. Optimized neutral structures do not show this special delocalization, instead predicting weakly bound molecular complexes. However, if the calculations are correct in predicting delocalization of the charge in the anionic complex into the n_p HOMO (b_2) or π^* (b_1) LUMO of formaldehyde, the singlet and triplet neutral electronic states accessed via photodetachment will be different from the optimized neutral structures.

We also consider an alternative explanation for the unique profile of the O_2^-·formaldehyde spectrum. In our previous study on O_2^-·[nonpolar VOC] complexes,[16] we reported an anomalous feature in the spectrum of O_2^-·benzene, the apparent dramatic enhancement of the transition to the a $^1\Delta_g$·[S_0] neutral state, with a more isotropic PAD. The e^-KE at which this enhancement was observed coincided with the e^-KE of a similar intensity anomaly in the O_4^-·benzene spectrum, and also coincided with a temporary anion state of benzene.[57] Formaldehyde has a temporary anion state at 0.86 eV, which corresponds to an e^-BE value of 2.63 eV with the photon energy used in this study.[58] Indeed, the area of enhanced signal with disparate PAD is at or above ca. 2.5 eV. We therefore measured the spectrum of O_4^-·formaldehyde, along with several other O_4^-·[polar VOC], to determine whether a broad feature would appear in the 0.5 to 1.2 eV e^-KE range, which would support the hypothesis of a temporary anion state of formaldehyde affecting the appearance of the spectrum.

Figure 7 shows the PE spectra of O_4^- and several O_4^-·[polar VOC] complexes. The direct detachment transitions, labeled X in all of the spectra, have very similar profiles. The O_4^- spectrum has been shifted to higher binding energy and superimposed onto the O_4^-·formaldehyde spectrum (dotted trace) to demonstrate the similarity of the two spectra.

The solvent shifts observed in the O_4^-·[polar VOC] complexes are in the range 0.6 eV for acetone to 0.9 eV for 3-buten-1-ol, lower than the solvent shifts observed in the O_2^-·

DOI: 10.1021/acs.jpca.7b05124
J. Phys. Chem. A 2017, 121, 5459−5467

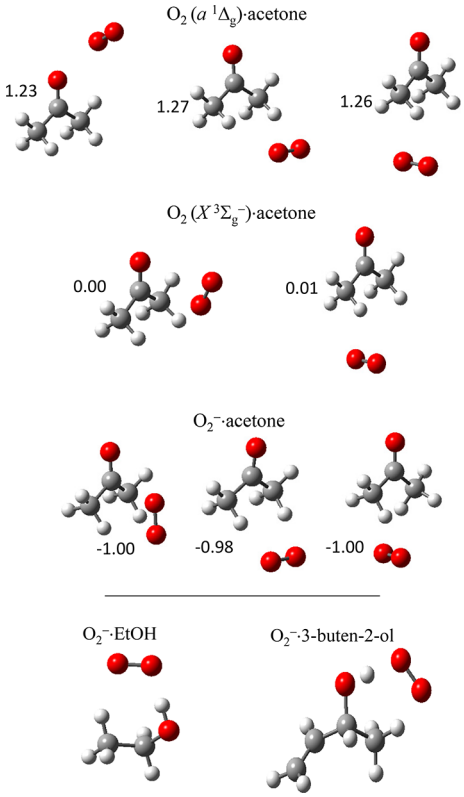

Figure 4. Structures of the O_2^-·acetone and O_2 ($X\ ^3\Sigma_g^-$)·acetone and O_2 ($a\ ^1\Delta_g$)·acetone complexes that converged in the calculations. In contrast to the several nearly isoenergetic structures found for O_2^-·acetone, alcohols are predicted to form a definitive structures in O_2^-·[polar VOC] complexes due to strong H-bonds with the hydroxyl group and the less conventional C−H H-bond with a β hydrogen.

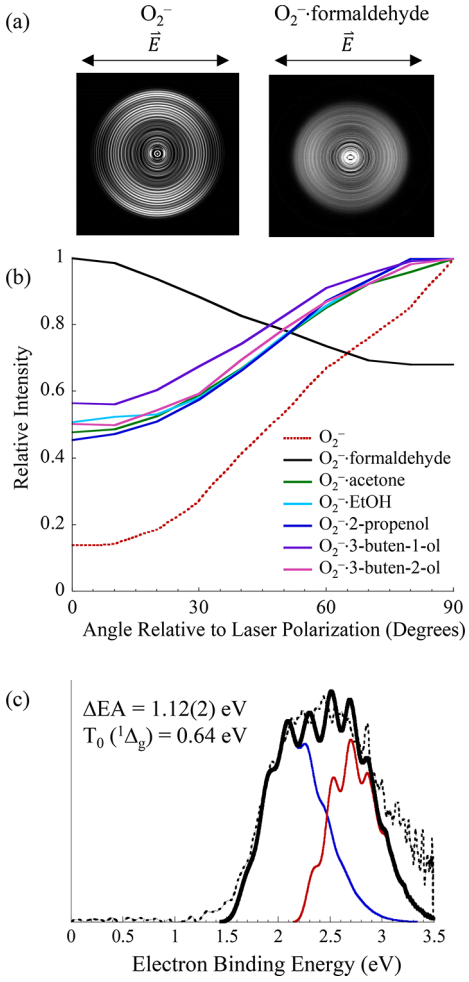

Figure 5. (a) Reconstructed PEIs of O_2^- and O_2^-·formaldehyde, (b) intensities of band X at the vertical detachment energy as a function of angle relative to the laser polarization, and (c) simulation of the O_2^-·formaldehyde PE spectrum. ΔEA is the energy difference between the origins of band X in the bare O_2^- simulation (Figure 3a) and the O_2^-·formaldehyde simulations. T_0 ($^1\Delta_g$) is the energy difference between the origins of the simulation of band a and the simulation of band X.

[polar VOC] spectra, which is consistent with charge being more delocalized on O_4^- than in O_2^- (or, larger ionic radius), resulting in weaker interactions in the complex. This effect is analogous to the solvation energy dependence on ionic radius in ionic solutions. We therefore suggest that the stronger O_2^-·formaldehyde interactions facilitate the orbital overlap leading to charge delocalization from O_2 into the molecular orbitals of formaldehyde, an effect that is turned off in the more weakly interacting O_4^-·formaldehyde complex.

Finally, features in the O_4^-·[polar VOC] spectra due to O_2^- autodetachment (O_2^- AD) and direct detachment (O_2^- DD) indicate that some photodissociation of the O_4^- moiety is occurring, along with direct detachment of the O_4^-·[polar VOC] complex. In the case of O_4^-·EtOH, signal from direct detachment of O_2^- is more prominent than in the other complex spectra, indicating both a larger photodissociation cross section and production of a larger proportion of the O_2^- photofragment with lower vibrational energy relative to O_4^-·[polar VOC] and O_4^-·[nonpolar VOC][16] complexes. Because the O_4^-·[polar VOC] complexes are not a focus of this study, we will not analyze this result further, and only comment on it because the appearance of this spectrum is notably different from the other O_4^- complex spectra.

IV. DISCUSSION

The interesting photophysics of O_2·**X** complexes can be largely attributed to the broken symmetry of the homonuclear O_2 molecular orbitals.[11−15] This broken symmetry is reflected in the PE spectra of and computational results on the O_2^-·[polar VOC] complexes in several ways.

First, PADs seen in the PEIs of the nonformaldehyde O_2^-·[polar VOC] complexes exhibit weaker polarization dependence than bare O_2^-, which can be interpreted as the result of the loss of the well-defined $|\lambda|$= 1 orbital angular momentum of the π_g orbitals yielding l = 0, 2 angular momentum photoelectrons. The interaction between O_2^- and the VOC will necessarily break the degeneracy of the π_g orbital, and results of calculations predict that the doubly occupied orbital in the O_2^- ($^2\Pi_g$)·[polar VOC] is the component pointing toward the molecule. As an example, the doubly occupied orbital predicted for the O_2^-·EtOH complex shown in Figure 6 maximizes the electron density for closest proximity to the dipole, allowing H-bonding (both via the conventional O---H−O hydrogen bond and the weaker O---H−C hydrogen bond). Detachment of the electron from the singly occupied orbital results in the neutral a $^1\Delta_g$·[polar VOC] with a structural arrangement that maintains electron density on the O_2 molecule closest to the hydroxyl hydrogen.

DOI: 10.1021/acs.jpca.7b05124
J. Phys. Chem. A 2017, 121, 5459−5467

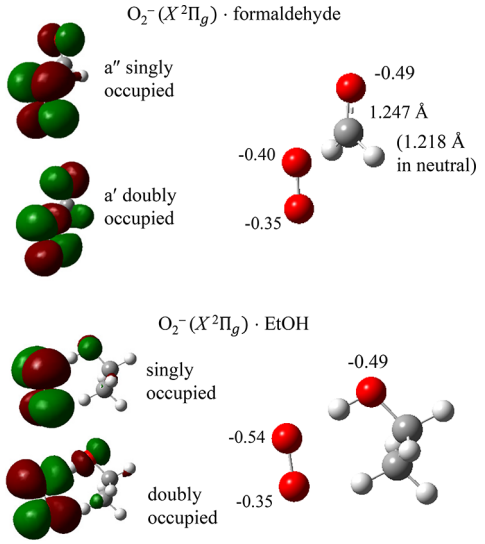

Figure 6. Depictions of the singly occupied HOMO and doubly occupied HOMO−1 from calculations on the O_2^-·formaldehyde compared to the those from the O_2^-·EtOH complex calculations, the latter of which are typical of the other complexes.

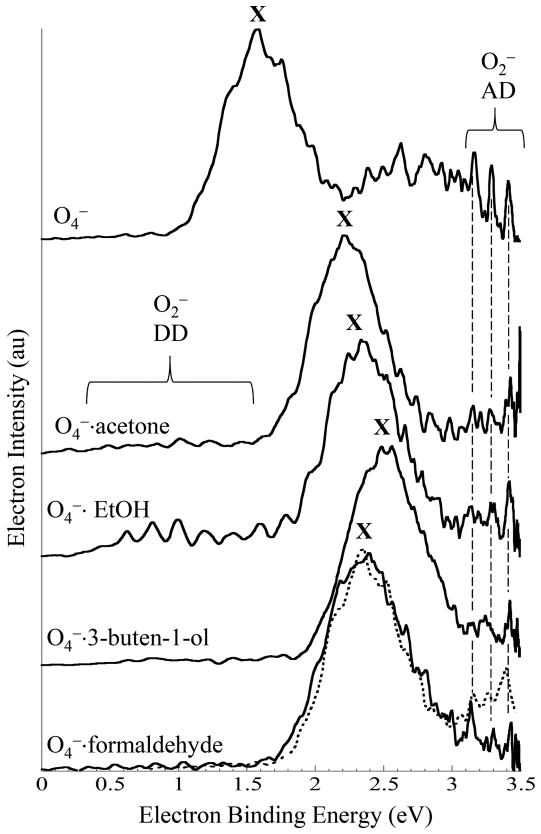

Figure 7. PE spectra of O_4^- and several O_4^-·[polar VOC] complexes obtained using 3.49 eV photon energy, illustrating that the O_4^-·formaldehyde complex spectrum does not exhibit the anomalous profile exhibited in the O_2^-·formaldehyde spectrum.

The calculated term energies of the various O_2 (a $^1\Delta_g$)·[polar VOC] states, summarized in Table 2, range between 1.19 and 1.28 eV, compared to 1.33 eV for bare O_2^- on the basis of single-point calculations, whereas the simulations support a larger stabilization of the O_2 (a $^1\Delta_g$)·[polar VOC] states relative to the O_2 (X $^3\Sigma_g^-$)·[polar VOC] states, ranging from 0.72 for O_2 (a $^1\Delta_g$)·3-buten-2-ol to 0.83 eV for O_2 (a $^1\Delta_g$)·acetone (experimental T_0 for bare O_2 is 0.9773 eV).[44] In addition to the modest reduction of the term energy for the singlet states in polar partner complexes, the structures of the O_2 (a $^1\Delta_g$)·[polar VOC] states are more similar to the anion, which would further decrease the energy difference between the VDEs of transitions to the O_2 (a $^1\Delta_g$)·[polar VOC] and O_2 (X $^3\Sigma_g^-$)·[polar VOC] states, due to a narrower Franck−Condon manifold of the former. One remaining question that would be addressed more appropriately with higher-level calculations is whether the detachment cross section for the transition to the O_2 (a $^1\Delta_g$)·[polar VOC] state is smaller than the cross section to the O_2 (X $^3\Sigma_g^-$)·[polar VOC] state. From a qualitative standpoint, the latter is accessed via detachment of an electron from the O_2^- π_g orbital oriented toward the H-bond and may therefore be more delocalized than the π_g perpendicular to the H-bond. The spatial delocalization of this orbital could increase the photodetachment cross section.

Finally, the O_2^-·formaldehyde complex is unique among this series: Though the shift in the electron binding energy is commensurate with the other O_2^-·[polar VOC] species in this study, the spectral profile and PAD are different. In the case of O_2^-·formaldehyde, the π_g orbitals are predicted to delocalize into the C−O π^* and n_p orbitals. The disparate PAD measured for the O_2^-·formaldehyde spectrum compared to the other PADs suggests that the electronic structure of the anion cannot be described qualitatively as O_2^-−local molecular orbitals weakly perturbed by the polar VOC partner. We note here that O_2^-·formaldehyde is isoelectronic with HO_2·formaldehyde complex,[59,60] the latter of which forms a peroxy−hydroxy complex. O_2^- is not abundant in the troposphere, so the findings here are not likely to have an impact on current models of tropospheric formaldehyde chemistry, but it does underscore the noninnocence of certain molecules in molecular clusters.

V. CONCLUSIONS

The PE spectra of O_2^-·[polar VOC] (VOC = acetone, ethanol, 2-propenol, 3-buten-1-ol, 3-buten-2-ol, and formaldehyde) were measured using photoelectron imaging and were analyzed by a combination of spectral simulations and MP2 calculations. The O_2^-·[polar VOC] (VOC = acetone, ethanol, 2-propenol, and 3-buten-1-ol) qualitatively resemble that of bare O_2^-, though shifted to higher e$^-$BE due to the enhanced stability of the anion relative to the neutral by the polar partner in the complex. Although acetone has a significantly higher dipole moment than the alcohols, the increase in e$^-$BE of the O_2^-·acetone complex relative to bare O_2^- is the smallest, underscoring particularly strong stabilization arising from the intimacy of hydrogen bonding in the complexes formed between O_2^- and the alcohols. On the basis of spectral simulations, the splitting between the neutral ground O_2 (X $^3\Sigma_g^-$)·[polar VOC] states and first excited O_2 (a $^1\Delta_g$)·[polar VOC] states (i.e., the term energy, T_0 of the singlet states) is lower than that of bare O_2 by 0.14−0.25 eV. This effect is attributed to the stabilization of the component of the broken degeneracy-π_g orbitals involved in hydrogen bonding or charge−dipole interactions in the anionic precursor. Band a in these spectra are less intense than band a in the bare O_2^- spectrum, which may be due to differences in photodetachment cross sections of no-longer-degenerate π_g orbitals.

DOI: 10.1021/acs.jpca.7b05124
J. Phys. Chem. A 2017, 121, 5459−5467

The spectrum of O_2^-·formaldehyde is qualitatively very different from the other complexes spectra in terms of both spectral profile and PAD. Calculations predict delocalization of charge from O_2^- into the HOMO and LUMO of formaldehyde, suggesting that formaldehyde is not an innocent polar partner in these complexes.

■ ASSOCIATED CONTENT

Supporting Information

The Supporting Information is available free of charge on the ACS Publications website at DOI: 10.1021/acs.jpca.7b05124.

Raw and reconstructed photoelectron images obtained with 3.49 eV photon energies of all species considered in this paper, slices through the reconstructed images obtained using 3.49 eV taken at 10° increments, and calculated molecular structures and relative energies for the various structures that converged in the calculations (PDF)

■ AUTHOR INFORMATION

Corresponding Author

*C. C. Jarrold. E-mail: cjarrold@indiana.edu. Phone: (812) 856-1190. Fax: (812)855-8300.

ORCID

Caroline Chick Jarrold: 0000-0001-9725-4581

Notes

The authors declare no competing financial interest.

■ ACKNOWLEDGMENTS

The authors gratefully acknowledge generous support for this work from the National Science Foundation, Grant Nos. CHE-1265991 and CHE-1664965.

■ REFERENCES

(1) Shardanand; Prasad Rao, A. D. Collision-Induced Absorption of O_2 in the Herzberg Continuum. *J. Quant. Spectrosc. Radiat. Transfer* **1977**, *17*, 433−439.

(2) Oshima, Y.; Okamoto, Y.; Koda, S. Pressure Effect of Foreign Gases on Herzberg Photoabsorption of Oxygen. *J. Phys. Chem.* **1995**, *99*, 11830−11833.

(3) Pfeilsticker, K.; Erle, F.; Platt, U. Absorption of Solar Radiation by Atmospheric O_4. *J. Atmos. Sci.* **1997**, *54*, 933−939.

(4) Zender, C. S. Global Climatology of Abundance and Solar Absorption of Oxygen Collision Complexes. *J. Geophys. Res.* **1999**, *104*, 24471−24484.

(5) Thalman, R.; Volkamer, R. Temperature Dependent Absorption Cross-Sections of O_2-O_2 Collision Pairs between 340 and 630 nm and at Atmospherically Relevant Pressure. *Phys. Chem. Chem. Phys.* **2013**, *15*, 15371−15381.

(6) Spiering, F. R.; van der Zande, W. J. Collision Induced Absorption in the $a^1\Delta(v = 2) \leftarrow X^3\Sigma_g^-$ (v = 0) Band of Molecular Oxygen. *Phys. Chem. Chem. Phys.* **2012**, *14*, 9923−9928.

(7) Richard, C.; Gordon, I. E.; Rothman, L. S.; Abel, M.; Frommhold, L.; Gustafsson, M.; Hartmann, J. M.; Hermans, C.; Lafferty, W. J.; Orton, G. S.; et al. New Section of the HITRAN Database: Collision-Induced Absorption (CIA). *J. Quant. Spectrosc. Radiat. Transfer* **2012**, *113*, 1276−1285.

(8) McKellar, A. R. W.; Rich, N. H.; Welsh, H. L. Collision-Induced Vibrational and Electronic Spectra of Gaseous Oxygen at Low Temperatures. *Can. J. Phys.* **1972**, *50*, 1−9.

(9) Long, C. A.; Ewing, G. E. The Infrared Spectrum of Bound State Oxygen Dimers in the Gas Phase. *Chem. Phys. Lett.* **1971**, *9*, 225−229.

(10) Long, C. A.; Ewing, G. E. Spectroscopic Investigation of van der Waals Molecules. 1. Infrared and Visible Spectra of $(O_2)_2$. *J. Chem. Phys.* **1973**, *58*, 4824−4834.

(11) Baklanov, A. V.; Bogomolov, A. S.; Pyryaeva, A. P.; Bogdanchikov, G. A.; Kochubei, S. A.; Farooq, Z.; Parker, D. H. Singlet Oxygen Photogeneration from X−O_2 van der Waals Complexes: Double Spin-flip vs. Charge-transfer Mechanism. *Phys. Chem. Chem. Phys.* **2015**, *17*, 28565−28573.

(12) Vidma, K. V.; Frederix, P.W.J.M.; Parker, D. H.; Baklanov, A. V. Photodissociation of van der Waals Clusters of Isoprene with Oxygen, C_5H_8−O_2, in the Wavelength Range 213−277 nm. *J. Chem. Phys.* **2012**, *137*, 054305.

(13) Baklanov, A. V.; Bogdanchikov, G. A.; Vidma, K. V.; Chestakov, D. A.; Parker, D. H. Cluster-Enhanced X-O_2 Photochemistry (X = CH_3O, C_3H_6, C_6H_{12}, and Xe). *J. Chem. Phys.* **2007**, *126*, 124316.

(14) Parsons, B. F.; Chandler, D. W. On the Dissociation of van der Waals Clusters of X_2 − Cyclohexane (X = 0, Cl) Following Charge-Transfer Excitation in the Ultraviolet. *J. Phys. Chem. A* **2003**, *107*, 10544−10553.

(15) DeBoer, G.; Young, M. A. Photochemistry and Dynamics of C_6H_6−O_2 Clusters at 266 nm. *J. Chem. Phys.* **1997**, *106*, 5468−5477.

(16) Patros, K. M.; Mann, J. E.; Jarrold, C. C. Photoelectron Imaging Spectra of O_2^-·VOC and O_4^-·VOC Complexes. *J. Phys. Chem. A* **2016**, *120*, 7828−7838.

(17) US EPA. *National-Scale Air Toxics Assessment*; U.S. Environmental Protection Agency: Washington, DC, 2011.

(18) Finlayson-Pitts, B. J.; Pitts, J. N. *Chemistry of the Upper and Lower Atmosphere: Theory, Experiments, and Applications*; Academic Press: San Diego, CA 2000.

(19) Steiner, A. L.; Cohen, R. C.; Harley, R. A.; Tonse, S.; Millet, D. B.; Schade, G. W.; Goldstein, A. H. VOC Reactivity in Central California: Comparing an Air Quality Model to Ground-Based Measurements. *Atmos. Chem. Phys.* **2008**, *8*, 351−368.

(20) Chatfield, R. B.; Ren, X.; Brune, W.; Schwab, J. Controls on Urban Ozone Production Rate as Indicated by Formaldehyde Oxidation Rate and Nitric Oxide. *Atmos. Environ.* **2010**, *44*, 5395−5406.

(21) Luecken, D. J.; Hutzel, W. T.; Strum, M. L.; Pouliot, G. A. Regional Sources of Atmospheric Formaldehyde and Acetaldehyde and Implications for Atmospheric Modeling. *Atmos. Environ.* **2012**, *47*, 477−490.

(22) Wang, X.; Wang, H.; Wang, S. Ambient Formaldehyde and its Contributing Factor to Ozone and OH Radical in a Rural Area. *Atmos. Environ.* **2010**, *44*, 2074−2078.

(23) Singh, H. B.; O'Hara, D.; Herlth, D.; Sachse, W.; Blake, D. R.; Bradshaw, J. D.; Kanakidou, M.; Crutzen, P. J. Acetone in the Atmosphere: Distribution, Sources, and Sinks. *J. Geophys. Res.* **1994**, *99*, 1805−1819.

(24) Jacob, D. J.; Field, B. D.; Jin, E. M.; Bey, I.; Li, Q.; Logan, J. A.; Yantosca, R. M. Atmospheric Budget of Acetone. *J. Geophys. Res.* **2002**, *107*, ACH5-1−ACH55-17.

(25) Raff, J. D.; Stevens, P. S.; Hites, R. A. Relative Rate and Product Studies of the OH − Acetone Reaction. *J. Phys. Chem. A* **2005**, *109*, 4728−4735.

(26) Farrell, A. E.; Plevin, R. J.; Turner, B. T.; Jones, A. D.; O'Hare, M.; Kammen, D. M. Ethanol Can Contribute to Energy and Environmental Goals. *Science* **2006**, *311*, 506−508.

(27) Jacobson, M. Z. Review of Solutions to Global Warming, Air Pollution, and Energy Security. *Energy Environ. Sci.* **2009**, *2*, 148−173.

(28) De Gouw, J. A.; Gilman, J. B.; Borbon, A.; Warneke, C.; Kuster, W. C.; Goldan, P. D.; Holloway, J. S.; Peischl, J.; Ryerson, T. B.; Parrish, D. D.; et al. Increasing Atmospheric Burden of Ethanol in the United States. *Geophys. Res. Lett.* **2012**, *39*, L15803.

(29) Jacobson, M. Z. Effects of Ethanol (E85) versus Gasoline Vehicles on Cancer and Mortality in the United States. *Environ. Sci. Technol.* **2007**, *41*, 4150−4157.

(30) Kirstine, W. V.; Galbally, I. E. The Global Atmospheric Budget of Ethanol Revisited. *Atmos. Chem. Phys.* **2012**, *12*, 545−555.

(31) Naik, V.; Fiore, A. M.; Horowitz, L. W.; Singh, H. B.; Wiedinmyer, C.; Guenther, A.; de Gouw, J. A.; Millet, D. B.; Goldan, P. D.; Kuster, W. C.; et al. Observational Constraints on the Global Atmospheric Budget of Ethanol. *Atmos. Chem. Phys.* **2010**, *10*, 5361−5370.
(32) Xu, Z.; Liu, Z.; Ge, M.; Wang, W. Uptake Kinetics of 3-buten-1-ol, 4-penten-1-ol and 3-methyl-3-buten-1-ol into Sulfuric Acid Solutions. *Chin. Sci. Bull.* **2011**, *56*, 1352−1356.
(33) Le Person, A.; Solignac, G.; Oussar, F.; Daële, V.; Mellouki, A.; Winterhalter, R.; Moortgat, G. K. Gas Phase Reaction of Allyl Alcohol (2-propen-1-ol) with OH Radicals and Ozone. *Phys. Chem. Chem. Phys.* **2009**, *11*, 7619−7628.
(34) Lee, A.; Goldstein, A. H.; Kroll, J. J.; Ng, N. L.; Varutbangkul, V.; Flagan, R. C.; Seinfeld, J. H. Gas-Phase Products and Secondary Aerosol Yields from the Photooxidation of 16 Different Terpenes. *J. Geophys. Res.* **2006**, *111*, D07302.
(35) Mann, J. E.; Troyer, M. E.; Jarrold, C. C. Photoelectron Imaging and Photodissociation of Ozonide in $O_3^- \cdot (O_2)_n$ (n = 1−4) Clusters. *J. Chem. Phys.* **2015**, *142*, 124305.
(36) Duncan, M. A. Infrared Laser Spectroscopy of Mass-Selected Carbocations. *J. Phys. Chem. A* **2012**, *116*, 11477−11491.
(37) Posey, L. A.; Deluca, M. J.; Johnson, M. A. Demonstration of a Pulsed Photoelectron Spectrometer on Mass-Selected Negative Ions: O^-, O_2^-, and O_4^-. *Chem. Phys. Lett.* **1986**, *131*, 170−174.
(38) Bakker, J. M. B. A Beam-Modulated Time-of-Flight Mass Spectrometer. I. Theoretical Considerations. *J. Phys. E: Sci. Instrum.* **1973**, *6*, 785−789.
(39) Bakker, J. M. B. A Beam-Modulated Time-of-Flight Mass Spectrometer. II. Experimental Work. *J. Phys. E: Sci. Instrum.* **1974**, *7*, 364−368.
(40) Eppink, A. T. J. B.; Parker, D. H. Velocity Map Imaging of Ions and Electrons Using Electrostatic Lenses: Application in Photoelectron and Photofragment Ion Imaging of Molecular Oxygen. *Rev. Sci. Instrum.* **1997**, *68*, 3477−3484.
(41) Chandler, D. W.; Houston, P. L. Two-Dimensional Imaging of State-Selected Photodissociation Products Detected by Multiphoton Ionization. *J. Chem. Phys.* **1987**, *87*, 1445−1447.
(42) Doyle, M. B.; Abeyasera, C.; Suits, A. G. *NuAcq 0.9: Native Megapixel Ion Imaging With Centroiding to 4 Mpix Using Inexpensive USB-2 Cameras*. Available at http://faculty.missouri.edu/suitsa/Technical_Resources.html.
(43) Dribinski, V.; Ossadtchi, A.; Mandelshtam, V. A.; Reisler, H. Reconstruction of Abel-Transformable Images: The Gaussian Basis-Set Expansion Abel Transform Method. *Rev. Sci. Instrum.* **2002**, *73*, 2634−2642.
(44) Ervin, K. M.; Anusiewicz, I.; Skurski, P.; Simons, J.; Lineberger, W. C. The Only Stable State of O_2^- Is the X $^2\Pi_g$ Ground State and It (Still!) Has an Adiabatic Electron Detachment Energy of 0.45 eV. *J. Phys. Chem. A* **2003**, *107*, 8521−8529.
(45) Garcia, G. A.; Nahon, L.; Powis, I. Two-dimensional Charged Particle Image Inversion Using a Polar Basis Function Expansion. *Rev. Sci. Instrum.* **2004**, *75*, 4989−4996.
(46) Frisch, M. J. T., Trucks, G. W.; Schlegel, H. B.; Scuseria, G. E.; Robb, M. A.; Cheeseman, J. R.; Scalmani, G.; Barone, V.; Mennucci, B.; Petersson, G. A.; et al. *Gaussian 09*, Revision A.1; Gaussian, Inc.: Wallingford, CT, 2009.
(47) Kendall, R. A.; Dunning, T. H.; Harrison, R. J. Electron Affinities of the First-Row Atoms Revisited. Systematic Basis Sets and Wave Functions. *J. Chem. Phys.* **1992**, *96*, 6796−6806.
(48) Jensen, F. *Introduction to Computational Chemistry*; Wiley: Chichester, England, Hoboken, NJ, 2007.
(49) Bogdanchikov, G. A.; Baklanov, A. V. Calculations of the Geometry and Binding Energy of the van der Waals Complex of Ethylene with Oxygen C_2H_4-O_2. *J. Struct. Chem.* **2015**, *56*, 983−988.
(50) Granucci, G.; Persico, M. Benzene-O_2 Interaction Potential from Ab Initio Calculations. *Chem. Phys. Lett.* **1993**, *205*, 331−336.
(51) Goebbert, D. J.; Sanov, A. Photodetachment, Photofragmentation, and Fragment Autodetachment of $[O_{2n}(H_2O)_m]^-$ Clusters: Core-Anion Structures and Fragment Energy Partitioning. *J. Chem. Phys.* **2009**, *131*, 104308.
(52) Kang, C.; Troyer, J. L.; Robertson, E. M.; Rothgeb, D. W.; Hossain, E.; Wyrwas, R. B.; Parmenter, C. S.; Jarrold, C. C. Solvation of O_2^- and O_4^- by *p*-diflurobenzene and *p*-xylene Studied by Photoelectron Spectroscopy. *J. Chem. Phys.* **2008**, *128*, 104309.
(53) Le Barbu, K.; Schiedt, J.; Weinkauf, R.; Schlag, E. W.; Nilles, J. M.; Xu, S.-J.; Thomas, O. C.; Bowen, K. H. Microsolvation of Small Anions by Aromatic Molecules: An Exploratory Study. *J. Chem. Phys.* **2002**, *116*, 9663−9671.
(54) Rosamonte's Physical Chemistry Website. Dipole Moment. https://physicalchemistryrosamonte.wordpress.com/material-balances/material-balances-on-a-crystallizer/physical-properties-of-pure-methanol/dipole-moment/ (Accessed Oct 20, 2016).
(55) Cooper, J.; Zare, R. N. Angular Distribution of Photoelectrons. *J. Chem. Phys.* **1968**, *48*, 942−943.
(56) Mabbs, R.; Mbaiwa, F.; Wie, J.; Van Duzor, M.; Gibson, S. T.; Cavanagh, S. J.; Lewis, B. R. Observation of Vibration-Dependent Electron Anisotropy in O_2^- Photodetachment. *Phys. Rev. A: At., Mol., Opt. Phys.* **2010**, *82*, 011401.
(57) Jordan, K. D.; Burrow, P. D. Studies of the Temporary Anion States of Unsaturated Hydrocarbons by Electron Transmission Spectroscopy. *Acc. Chem. Res.* **1978**, *11*, 341−348.
(58) Burrow, P. D.; Michejda, J. A. Electron Transmission Study of the Formaldehyde Electron Affinity. *Chem. Phys. Lett.* **1976**, *42*, 223−226.
(59) Morajkar, P.; Schoemaecker, C.; Okumura, M.; Fittschen, C. Direct Measurement of the Equilibrium Constants of the Reaction of Formaldehyde and Acetaldehyde with HO_2 Radicals. *Int. J. Chem. Kinet.* **2014**, *46*, 245−259.
(60) Anglada, J. M.; Domingo, V. M. Mechanism for the Gas-Phase Reaction between Formaldehyde and Hydroperoxyl Radical. A Theoretical Study. *J. Phys. Chem. A* **2005**, *109*, 10786−10794.

DOI: 10.1021/acs.jpca.7b05124
J. Phys. Chem. A 2017, 121, 5459−5467